

The magnetic field induced ferromagnetism in EuPd_2Sn_4 novel compound

I Čurlík¹, M Zapotoková¹, F Gastaldo², M Reiffers^{1,3}, J G Sereni⁴, M Giovannini²

¹Faculty of Humanities and Natural Sciences, University of Prešov, 17. novembra 1, Prešov, Slovakia

²Department of Chemistry, University of Genova, Via Dodecaneso 31, Genova, Italy

³Institute of Experimental Physics, Slovak Academy of Science, Watsonova 47, Košice, Slovakia

⁴Department of Physics, CAB-CNEA, CONICET, IB-UNCuyo, 8400 S. C. de Bariloche, Argentina

E-mail: ivan.curlik@unipo.sk

Abstract. We report on crystal structure, magnetic and thermal physical properties of EuPd_2Sn_4 stannide. From the magnetic susceptibility measurements a divalent state of Eu rare earth element was determined together with an antiferromagnetic (AFM) order at 11 K. By applying magnetic field, the magnetic behavior variation reveals a complex magnetic structure. Above a critical field B_c a ferromagnetic (FM)-like character starts to prevail. AFM and FM regimes are separated by a metamagnetic region. Heat capacity measurements confirm this behavior.

Keywords: europium, AFM, FM, metamagnetism

1. Introduction

Eu, as well as Sm, Tm, Yb and Ce intermetallic compounds constitute an interesting class of materials, owing to different configuration of their $4f$ -electrons which can lead to the phenomenon of valence instability where valence fluctuates between integer values [1].

In the last years we have carried out a systematic investigation on $R\text{-Pd-}X$ ($R = \text{Eu, Yb, Ce}$; $X = \text{In, Sn}$) ternary compounds among which a certain number of them exhibited anomalous physical behaviour [2, 3, 4, 5].

Concerning the Eu-Pd-Sn system, novel compounds have been discovered, such as $\text{Eu}_3\text{Pd}_2\text{Sn}_2$ and EuPdSn_2 , showing a stable Eu^{2+} magnetic state and complex magnetic structures [6, 7, 8]. This last feature, together with a magnetic anisotropy, seems to characterize many compounds belonging to $\text{Eu-}T\text{-}X$ systems ($T =$ transition metals; $X = p\text{-block elements}$). In fact, magnetic properties measured on a single crystal of EuRh_2Si_2 exhibit a marked magnetic anisotropy with the easy plane perpendicular to the c axis [9], whereas a single crystal study on EuRhGe_3 revealed significant anisotropy and incommensurate antiferromagnetic structures with amplitude-modulated character [10]. These elaborated magnetic scenarios require to be verified by microscopic techniques, like neutron diffraction. A careful neutron scattering study was indeed performed on EuPdSn , confirming the complex magnetic structure occurring in these compounds. In fact, EuPdSn exhibits a non collinear sine-wave modulated structure below $T = 15.5$ K which evolves into a planar helimagnetic structure at lower temperatures [11].

These scenarios of complex and strongly anisotropic magnetism are not expected for Eu^{2+} because of its spin $S = 7/2$ and orbital $L = 0$ numbers precluding the presence of crystal electric field effects.

Following the same line of study of Eu-based compounds, in this work we report on the physical properties of EuPd_2Sn_4 , a new ternary member of the Eu-Pd-Sn system.

2. Experimental details

EuPd_2Sn_4 polycrystalline sample has been prepared by weighing the stoichiometric amount of elements with the following nominal purity: Eu – 99.99 mass % (pieces, Smart Elements GmbH, Vienna, Austria), Pd – 99.95 mass % (foil, Chimet, Arezzo, Italy), Sn – 99.999 mass % (bar, Smart Elements GmbH, Vienna, Austria). Due to Eu element being prone to high oxidation reaction on air, the EuPd_2Sn_4 sample has been weighed inside a glove box. In order to avoid the loss of europium during the melting because of its high vapour pressure, all the weighed elements (in total weight of 1.2 g) were enclosed in a small tantalum crucible sealed by arc welding in an inert atmosphere inside the glove box.

The sample was subsequently melted in an induction furnace under a stream of pure argon. To ensure homogeneity, the crucible was continuously shaken during the melting. Sample was then annealed in a resistance furnace for two weeks at the temperature of 600 °C and finally quenched in cold water.

The sample was characterized by scanning electron microscopy (EVO 40, Carl Zeiss, Cambridge, England) equipped with quantitative electron probe microanalysis system based on energy dispersive X-ray spectroscopy (EPMA - EDXS). For the quantitative and qualitative analysis an acceleration voltage of 20 keV for 100 s was applied, and a cobalt standard was used for calibration. The crystal

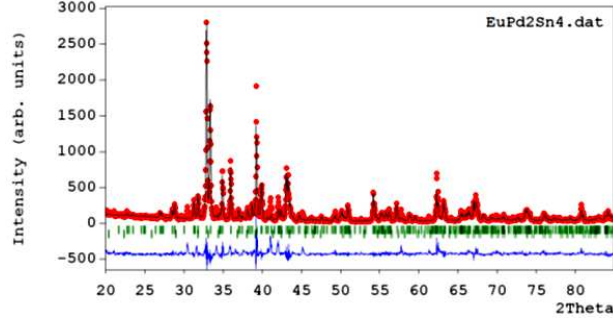


Figure 1. X-ray diffraction powder pattern of EuPd_2Sn_4 . The experimental data are shown with circle symbols, while the solid line through the experimental points represents Rietveld refinement. The indexed peaks associated to the crystal structure of EuPd_2Sn_4 are displayed with the upper ticks (lower ticks indicate traces of $\text{Eu}_3\text{Pd}_4\text{Sn}_{13}$). The lower curve represents the difference curve.

structure was determined by powder X-ray diffraction (XRD) using the vertical diffractometer X/Pert MPD (Philips, Almelo, The Netherlands) equipped with a graphite monochromator installed in the diffraction beam (Bragg Brentano, $\text{Cu K}\alpha$ radiation). The theoretical powder pattern was calculated with the help of the Powder-Cell software [12] and for Rietveld refinements the FULLPROFF program was used [13].

The thermodynamic and magnetic physical properties measurements were performed using a Physical Property Measurement System Dynacool (Quantum Design) in the temperature range of 2 – 400 K under applied magnetic field up to 9 T. Specific heat was determined by means of the relaxation $2\text{-}\tau$ method.

3. Experimental results

3.1. Crystal structure analysis

From SEM/EPMA analyses the sample prepared on nominal composition EuPd_2Sn_4 resulted to be almost single phase with some traces of $\text{Eu}_3\text{Pd}_4\text{Sn}_{13}$ (crystallizing in the $\text{Yb}_3\text{Rh}_4\text{Sn}_{13}$ structure type) and an unknown phase of atomic composition 5 % Eu, 40 % Pd, 55 % Sn.

The XRD pattern of the EuPd_2Sn_4 phase (shown in Fig. 1) was successfully indexed by analogy with the corresponding already known orthorhombic phase NdAu_2In_4 [14], which crystallizes in NdRh_2Sn_4 -structure type ($oP28$) [15]. Its crystal structure was established as orthorhombic, space group $Pnma$ (Nº. 62).

The atomic positions of NdAu_2In_4 were taken as starting values and structure was successfully refined in the XRD dataset by using FULLPROF software [13]. The refined lattice parameters for EuPd_2Sn_4 are: $a = 1.8659(7)$ nm, $b = 0.4600(6)$ nm, $c = 0.7284(5)$ nm. The details of the structural atomic coordinates of EuPd_2Sn_4 are reported in Tab. 1. A final reliability factor of $R_p = 22.6$ % and $\chi^2 = 3.71$ were obtained in the Rietveld refinement (see Fig. 1).

Table 1. Atomic fractional coordinates of the novel compound EuPd_2Sn_4 .

Atom	Wyckoff position	x/a	y/b	z/c
Sn1	4c	0.0316(3)	1/4	0.366(1)
Sn2	4c	0.1817(4)	1/4	0.816(1)
Sn3	4c	0.1966(5)	1/4	0.235(1)
Sn4	4c	0.4327(4)	1/4	0.486(1)
Pd1	4c	0.0346(5)	1/4	0.741(1)
Pd2	4c	0.2913(5)	1/4	0.538(1)
Eu	4c	0.3601(5)	1/4	0.009(1)

3.2. Magnetic properties

Fig. 2 shows the temperature dependence of the inverse magnetic susceptibility $1/\chi(T)$ of EuPd_2Sn_4 in the temperature range of 2 – 400 K measured in the applied magnetic field of 1 T. The compound exhibits Curie-Weiss (CW) behaviour above 11 K. To evaluate the basic magnetic characteristics we fitted $1/\chi(T)$ dependence in this temperature range following the equation

$$1/\chi(T) = \left[\chi_0 + \frac{C}{T - \Theta_P} \right]^{-1} \quad (1)$$

where χ_0 , C and Θ_P represent the Pauli susceptibility, Curie constant and paramagnetic Curie temperature, respectively. The obtained value of the effective magnetic moment $\mu_{eff} = 7.95 \mu_B$ is close to the theoretical Eu^{2+} free ion value ($7.94 \mu_B$) indicating that Eu ions are in the magnetic state. The small but positive value of the paramagnetic Curie temperature $\theta_P = 4.98$ K denotes some ferromagnetic (FM) exchange interactions between magnetic moments. The Pauli susceptibility χ_0 obtained from the fit is negligible ($\sim 10^{-10} \text{ m}^3\text{mol}^{-1}$). For comparison, we fitted also the $1/\chi(T)$ dependence in applied magnetic field 9 T. The resulting values ($\theta_P = 3.34$ K, $\mu_{eff} = 7.98 \mu_B$) reveal negligible changes in comparison to those obtained from measurements in 1 T.

The inset of Fig. 2 presents the low temperature details of the $\chi(T)$ dependence of EuPd_2Sn_4 with a peak at $T_N = 11$ K indicating a phase transition from paramagnetic to magnetically ordered state. Notably, such a sharp cusp is characteristic for antiferromagnetic (AFM) ordering. As one can see there is no obvious difference between zero field cooling (ZFC) and field cooling (FC) dependencies (in analogy with the results observed in EuPdSn_2 [8]) suggesting an AFM order. However, taking into account the positive θ_P value, a more complex magnetic structure can not be excluded. Complex magnetic structures were already described in EuPdSn , where neutron diffraction experiment revealed incommensurate magnetic structures (sinusoidally modulated vs. planar helimagnetic) in different temperature ranges well below the T_N transition [11].

In order to proceed with a detailed investigation of the ground-state magnetic properties of EuPd_2Sn_4 , a series of $\chi(T)$ measurements were performed focusing to the low temperature range between 2 – 30 K in different applied magnetic fields up to 9 T. The $\chi(T)$ dependencies were measured in FC regime where magnetic field was gradually increased by steps of 0.05 T for every consecutive measurement. Resulted dependencies are presented on *a* and *b* panels of Fig. 3. For applied fields up to around 1 T, $\chi(T)$ shows a cusp characteristic for AFM ordering (the blue curves in Fig. 3a).

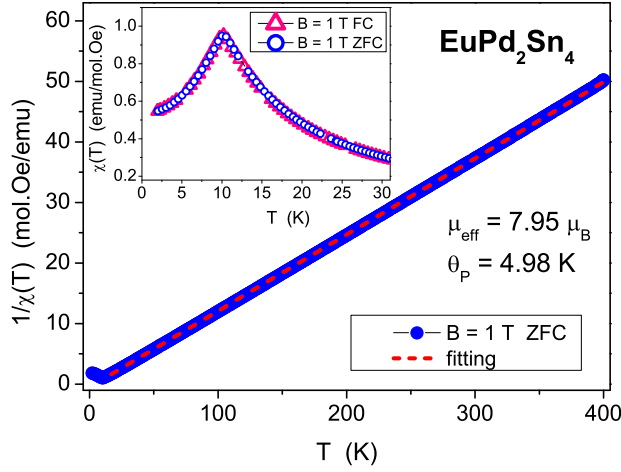


Figure 2. Temperature dependence $1/\chi(T)$ for EuPd_2Sn_4 compound measured in the temperature range 2 – 400 K in applied magnetic field of 1 T. In the inset the $\chi(T)$ dependence in the temperature range 2 – 30 K with the maximum at 11 K is shown.

With increasing B up to 2 T, the transition temperature T_N shifts to lower values and the peak broadens. For $B > 2$ T the $\chi(T)$ dependencies change their character, the AFM maximum disappears and $\chi(T)$ continuously increases with lowering the temperature (black curves on Fig. 3b). The displayed set of $\chi(T)$ measurements shows the trend of magnetic saturation effect with increasing B . It seems that FM-like correlations become prevalent in the system. This could explain also the positive θ_P calculated from the fitting. Within the B range of $\approx 2 - 2.3$ T (red curves in both a, b panels of Fig. 3) the absolute values of $\chi(T)$ measurements are progressively higher and this is typical for a progressive FM field induced alignment from an AFM state. A similar switching of prevailing type of magnetic interactions between AFM and FM was found in EuPdSn_2 measurements [8], whereas antiferromagnetic EuRh_2Si_2 was found to be on the verge of ferromagnetism above barely 0.1 T [16, 17].

This scenario of field-induced ferromagnetism in EuPd_2Sn_4 is corroborated by the $M(B)$ magnetization dependencies at temperatures from 2 to 100 K (Fig. 4). In the $M(B)$ isotherms measured above the ordering temperature $T_N = 11$ K, the curves show the typical field dependence described by a Brillouin function expected for a paramagnetic compound, whereas below T_N a metamagnetic-like behavior in the $M(B)$ takes place for the values of critical magnetic field B_c between 1 and 2 T. The B_c was evaluated as the maximum of dM/dB derivative (see the inset of Fig. 4), which represents the magnetic field for which the AFM regime is destroyed and the metamagnetic processes predominate. The inset of Fig. 4 shows the maxima corresponding to B_c for different $M(B)$ isotherms where, with increasing temperature, B_c assumes smaller values (depicted later in Fig. 6 with orange pentagons). Far above the metamagnetic transition at $B = 9$ T and $T = 2$ K the magnetization saturates at $6.95 \mu_B/\text{Eu}$ which is very close to the free Eu^{2+} saturation moment $gJ = 7 \mu_B/\text{Eu}$.

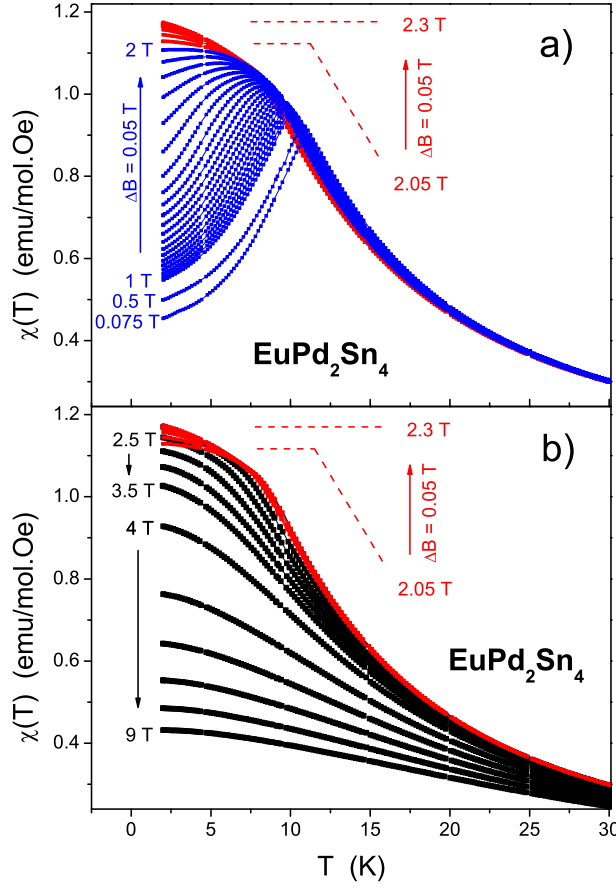


Figure 3. Set of temperature dependent $\chi(T)$ susceptibilities for EuPd_2Sn_4 compound measured in the temperature range 2 – 30 K in magnetic fields within the range 0.075 – 2.3 T (panel a) and 2.05 – 9 T (panel b). According to the characteristic AFM/FM-like shape, the $\chi(T)$ dependencies are depicted on the corresponding a/b panel of the figure.

3.3. Specific heat

The specific heat $C_p(T)$ of EuPd_2Sn_4 in the temperature range 2 – 230 K for zero magnetic field is reported in the inset of Fig. 5. In the low temperature region a λ -anomaly at ≈ 11 K is observed, indicating the transition into AFM state. The main panel of Fig. 5 presents the detail of this anomaly in accordance to different applied magnetic fields up to 9 T. For magnetic field $B < 2$ T the $C_p(T_N)$ jump starts being reduced both in the temperature and the height. This behavior is a typical feature of antiferromagnetically ordered systems in agreement with the $\chi(T)$ results (see Fig. 3). In comparison with the magnetic measurements, the T_N values extracted from $C_p(T)$ dependencies equally match with the Néel temperatures obtained from the $\chi(T)$ and tends to the same AFM trend below B_c . The $C_p(T)$ dependencies on Fig. 5 also confirm the progressive FM-like character for $B > 2.5$ T where the maximum shifts to higher T and broadens with the strength of B (characteristic for FM polarization). At lower temperature (around 5 K) a shoulder-like anomaly is observed. Such a broad

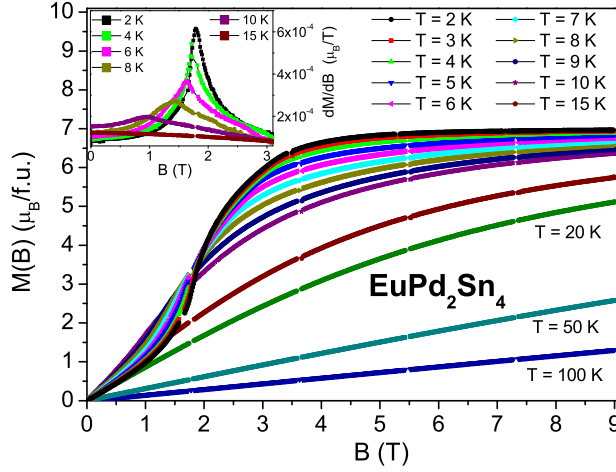


Figure 4. Isothermal $M(B)$ magnetization of EuPd_2Sn_4 for the magnetic field 0 – 9 T measured at selected temperatures within the range 2 – 100 K. Inset of the figure shows the field dependencies of dM/dB derivative in the 0 – 3 T range for selected isotherms.

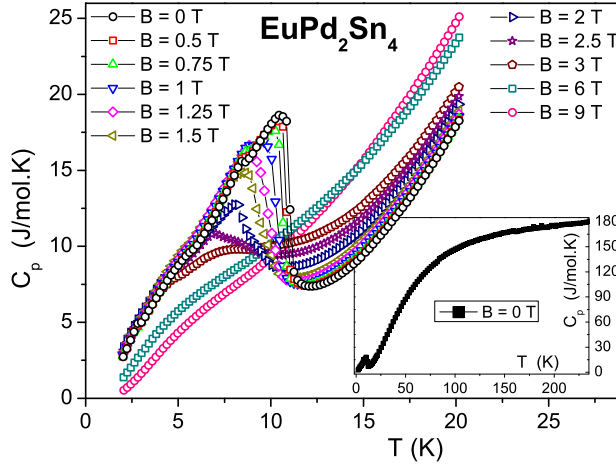


Figure 5. Low temperature dependence of specific heat $C_p(T)$ of EuPd_2Sn_4 in different magnetic field from the range 0 – 9 T. The inset presents the $C_p(T)$ measurements in zero field up to high temperatures.

shoulder, seen around $1/4$ of T_N , is typical for $4f^7$ systems (Eu^{2+} and Gd^{3+}) and is related to the large degeneracy of the $J = 7/2$ local moment within the mean-field theory for a $(2J + 1)$ -fold degenerate multiplet [8, 17, 18].

3.4. Magnetic phase diagram

Fig. 6 presents the analysis of the transition temperature as a function of applied magnetic field from the series of $\chi(T)$ curves (Fig. 3), $M(B)$ magnetization (Fig. 4) and the $C_p(T)$ specific heat measurements (Fig. 5). For values of magnetic field ranging from zero up to ≈ 2 T the T_N values, taken from maxima of $\chi(T)$ curves,

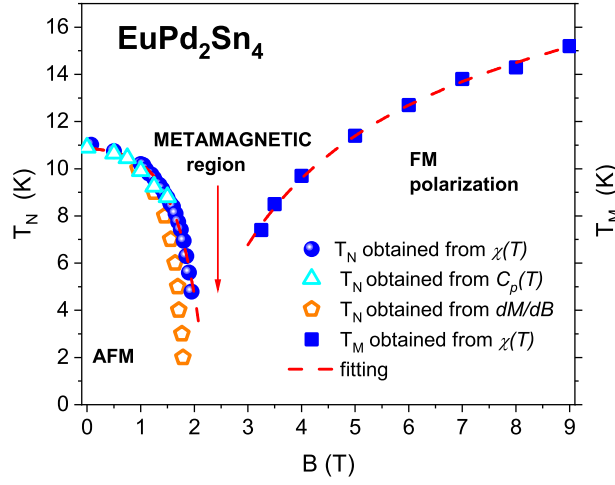


Figure 6. The magnetic phase diagram shows the variation of transition temperature T_N and characteristic temperature T_M as a function of external magnetic field B . The graphics displays the variation of dominant magnetic interactions in EuPd_2Sn_4 as a function of applied magnetic field.

decrease in agreement with typical AFM ordering (blue circles). The same trend of T_N variation with magnetic field results from the analysis of $C_p(T)$ dependencies measured at $B \leq 1.5$ T (cyan triangles). For magnetic fields above 2.5 T, the magnetic evolution of the system can be described tracing the temperature of the maximum $d\chi/dT$ slope: $T_{M(B)} = (d\chi/dT)_{max}$ (blue squares in Fig. 6). This field induced ferromagnetic behaviour is consistent with the isothermal $M(B)$ magnetization measurements (inset of Fig. 4), where the critical magnetic field B_c was evaluated for different temperatures. In Fig. 6 we present this T_N vs. B_c dependence (orange pentagons). The graphics is divided in two areas depending on the dominating type of interaction (AFM vs FM). On the magnetic field axis the AFM/FM-like regimes are separated by the region of metamagnetic behaviour left bounded by the critical magnetic field B_c . Such an explanation congruent with the $\chi(T)$ susceptibility (Fig. 3) and $M(B)$ magnetization (Fig. 4) measurements is supported also by the results for the analogous system – EuPtIn where two metamagnetic transitions between AFM and FM spin alignment were observed [19].

4. Conclusions

The EuPd_2Sn_4 compound has been synthesised by induction melting, and magnetic and thermal physical properties have been studied. In this stannide Eu was found in divalent state, which makes EuPd_2Sn_4 a magnetic compound. The series of $\chi(T)$ magnetic susceptibilities measured in low magnetic field reveal an antiferromagnetic ordering at 11 K, but increasing the strength of B a more complex magnetic nature was observed. A typical AFM ground state was observed for values lower than $B < 2$ T and a further increase of magnetic field induces FM-like behaviour. These two regimes are separated by a metamagnetic region revealed by $M(B)$ measurements. The complexity and variation of magnetic mechanisms in EuPd_2Sn_4 are supported by specific heat experiment where $C_p(T)$ dependencies in $B > 2.5$ T are characterized by field induced

FM behaviour, possibly due to a non-collinear ordering of magnetic moments in AFM state. As a consequence, the increasing of magnetic field B would cause the rearrangement of magnetic moments towards a FM-like state. However, a change in the magnetic structure should be confirmed by neutron powder diffraction measurements.

Acknowledgments

Acknowledgements This work was supported by the projects VEGA 1/0956/17, VEGA 1/0611/18, VEGA 1/0705/20 and APVV-16-0079, University Science Park TECHNICOM for Innovation Applications Supported by Knowledge Technology - II. phase (ITMS: 313011D232), Research & Development Operational Programme funded by the ERDF.

References

- [1] Lawrence J M, Riseborough P S and Parks R D 1981 *Reports on Progress in Physics* **44** 1–84
- [2] Muramatsu T, Kanemasa T, Kagayama T, Shimizu K, Aoki Y, Sato H, Giovannini M, Bonville P, Zlatić V, Aviani I, Khasanov R, Rusu C, Amato A, Mydeen K, Nicklas M, Michor H and Bauer E 2011 *Physical Review B* **83** ISSN 1098-0121
- [3] Giovannini M, Pasero R and Saccone A 2010 *Intermetallics* **18** 429 – 433
- [4] Sereni J G, Giovannini M, Berisso M G and Saccone A 2011 *Physical Review B* **83**
- [5] Martinelli A, Sanna S, Lamura G, Ritter C, Joseph B, Bauer E and Giovannini M 2019 *Journal of Physics: Condensed Matter* **31**
- [6] Solokha P, Čurlík I, Giovannini M, Lee-Hone N, Reiffers M, Ryan D and Saccone A 2011 *Journal of Solid State Chemistry* **184** 2498–2505
- [7] Čurlík I, Gastaldo F, Giovannini M, Strydom A and Reiffers M 2017 *Acta Physica Polonica A* **131** 1003–1005
- [8] Čurlík I, Giovannini M, Gastaldo F, Strydom A M, Reiffers M and Sereni J G 2018 *Journal of Physics: Condensed Matter* **30** 495802
- [9] Seiro S and Geibel C 2013 *Journal of Physics: Condensed Matter* **26** 046002
- [10] Bednarchuk O and Kaczorowski D 2015 *Journal of Alloys and Compounds* **646** 291 – 297 ISSN 0925-8388
- [11] Lemoine P, Cadogan J M, Ryan D H and Giovannini M 2012 *Journal of Physics: Condensed Matter* **24** 236004
- [12] Kraus W and Nolze G 1996 *Journal of Applied Crystallography* **29** 301–303
- [13] Rodríguez-Carvajal J 1993 *Physica B: Condensed Matter* **192** 55 – 69 ISSN 0921-4526
- [14] Salvador J R, Hoang K, Mahanti S D and Kanatzidis M G 2007 *Inorganic Chemistry* **46** 6933–6941
- [15] Méot-Meyer M, Venturini G, Malaman B and Roques B 1985 *Materials Research Bulletin* **20** 913 – 919 ISSN 0025-5408
- [16] Hossain Z, Trovarelli O, Geibel C and Steglich F 2001 *Journal of Alloys and Compounds* **323–324** 396 – 399 ISSN 0925-8388 proceedings of the 4th International Conference on f-Elements
- [17] Seiro S and Geibel C 2011 *Journal of Physics: Condensed Matter* **23** 375601
- [18] Bednarchuk O and Kaczorowski D 2015 *Acta Physica Polonica A* **127** 418 – 420
- [19] Müllmann R, Mosel B D, Eckert H, Kotzyba G and Pöttgen R 1998 *Journal of Solid State Chemistry* **137** 174 – 180 ISSN 0022-4596